ACS APPLIED MATERIALS & INTERFACES

www.acsami.org

Research Article

Controllable Plexcitonic Coupling in a WS_2-Ag Nanocavity with Solvents

Xiaobo Han, Kai Wang,* Yanan Jiang, Xiangyuan Xing, Shujin Li, Huatian Hu, Weiwei Liu, Bing Wang, and Peixiang Lu*

Cite This: https://doi.org/10.1021/acsami.1c10295

Read Online

ACCESS | Metrics & More | Article Recommendations | Supporting Information

ABSTRACT: Strong coupling between emitters and cavities underlies many of the current strategies aiming at generating and controlling quantum states at room temperature. Recent experiments reveal strong coupling between two-dimensional transition metal dichalcogenides (TMDCs) and individual plasmonic structures; however, the coupling strength is quite limited (<200 meV), and the active control of the coupling strength is challenging. Here, we demonstrate the active tuning of plexcitonic coupling in monolayer WS_2 coupled to a plasmonic nanocavity by immersing into a mixed solution of dichloromethane (DCM) and ethanol. By adjusting the mixture ratio, continuous tuning of the Rabi splitting energy ranged from 183 meV (in ethanol) to 273 meV (in DCM) is achieved. The results are mainly attributed to the remarkable increase of the neutral exciton density in monolayer WS_2 as the concentration of DCM is increased. It offers an important stepping stone toward a further study on plexcitonic coupling in layered materials, along with potential applications in quantum information processing and nonlinear optical materials.

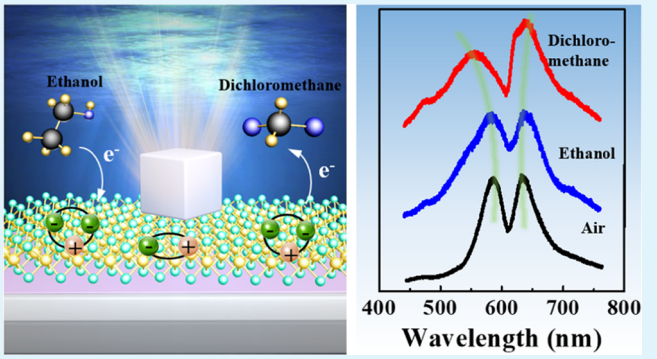

KEYWORDS: *strong coupling, WS_2 monolayer, transition metal dichalcogenides, plasmonic nanocavity, electron transfer*

1. INTRODUCTION

Light−matter interactions are essential to many contemporary scientific disciplines.[1−3] A special interaction regime called strong coupling[4−7] is achieved when the rate of coherent energy exchange between an emitter and a cavity exceeds their intrinsic dissipation rates. Layered materials, in particular, two-dimensional transition metal dichalcogenides (TMDCs) possessing a huge dipole moment, attract much interest in the research of strong light−matter interactions.[8] Recently, several studies demonstrate strong plasmon−exciton (plexcitonic) coupling between TMDCs and plasmonic nanostructures. Although TMDCs provide a better platform for realizing strong coupling at room temperature than quantum dots (QDs) and J-aggregates, the observed Rabi splitting (RS) energy is quite limited (<200 meV).[9−17] The largest RS energies are obtained to be 163 and 175 meV in mono-[16] and multilayer TMDCs,[17] respectively, coupled to plasmonic nanostructures, which are still smaller than that in the J-aggregate system (typical value ∼400 meV).[18,19] Therefore, it is essential to enhance plexcitonic coupling strength in TMDCs/plasmonic nanocavity.

On the other hand, the continuous control of the strong coupling strength is highly desirable for a versatile coupling system with precisely tailored optical responses.[20] As recently reported, it has been demonstrated in TMDCs/plasmonic nanocavity with electric tuning.[21,22] However, the reported strong coupling strength is limited to ∼60 meV, while it can only be turned down to the weak coupling regime. Therefore, it is quite a challenging task to tune the plexcitonic coupling with enhanced coupling strength in TMDCs/plasmonic nanostructures. In general, it is the neutral exciton that interacts with the surface plasmon for strong coupling.[9−17] Excitingly, excitons in TMDCs are proved to be reversibly converted from trions in TMDCs by chemical doping[23] and solvent effects.[24,25] Furthermore, the transition dipole moment in solvent-immersed TMDCs is also increased, which is conducive to enhancing the strong coupling strength. Therefore, it is expected to enhance and tune the coupling strength by manipulating excitons in TMDCs under immersion in different solvents.

In this work, we demonstrate exciton manipulation of plexcitonic coupling in a monolayer WS_2-Ag nanocavity by immersing into the mixed solution of dichloromethane

Received: June 3, 2021
Accepted: August 20, 2021

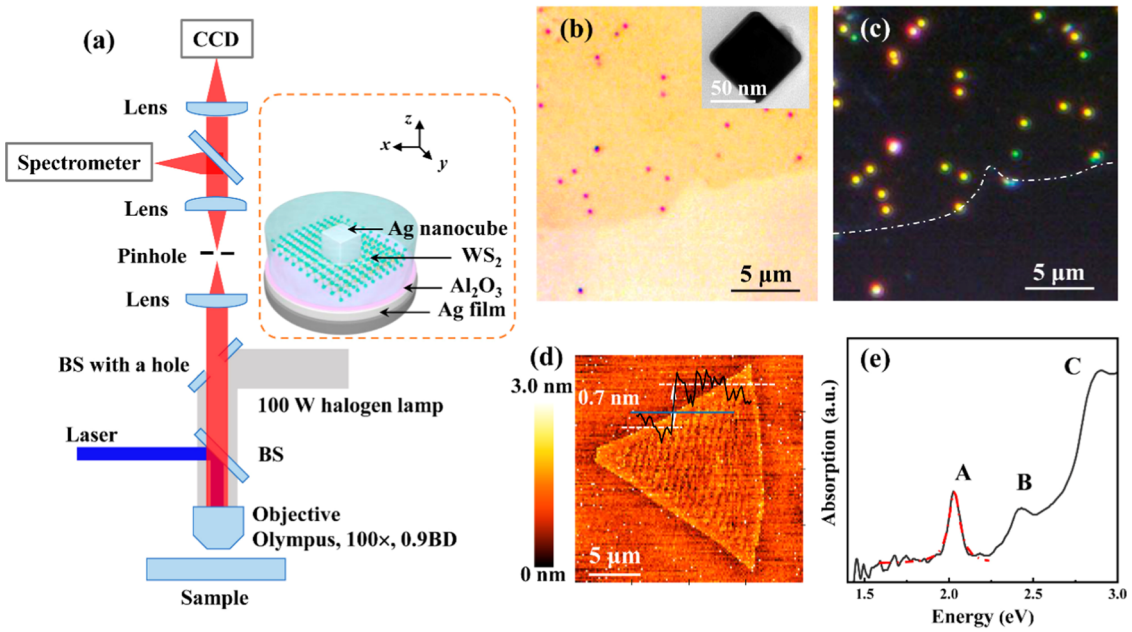

Figure 1. (a) Experimental setup for measuring single hybrids. BS indicates beam splitting. Inset: scheme of a WS_2-Ag nanocavity immersed in a solvent. (b, c) Bright-field and DF images of the hybrids. Inset of (b): TEM image of the Ag nanocube. The white dash line in (c) marks the edge of WS_2. (d) AFM image of a WS_2 flake grown on the sapphire substrate. Inset: AFM height profile indicated by the blue line. (e) Measured absorption spectrum of monolayer WS_2 on the sapphire in air (black curve). The red curve is the single-peak Lorentz fit.

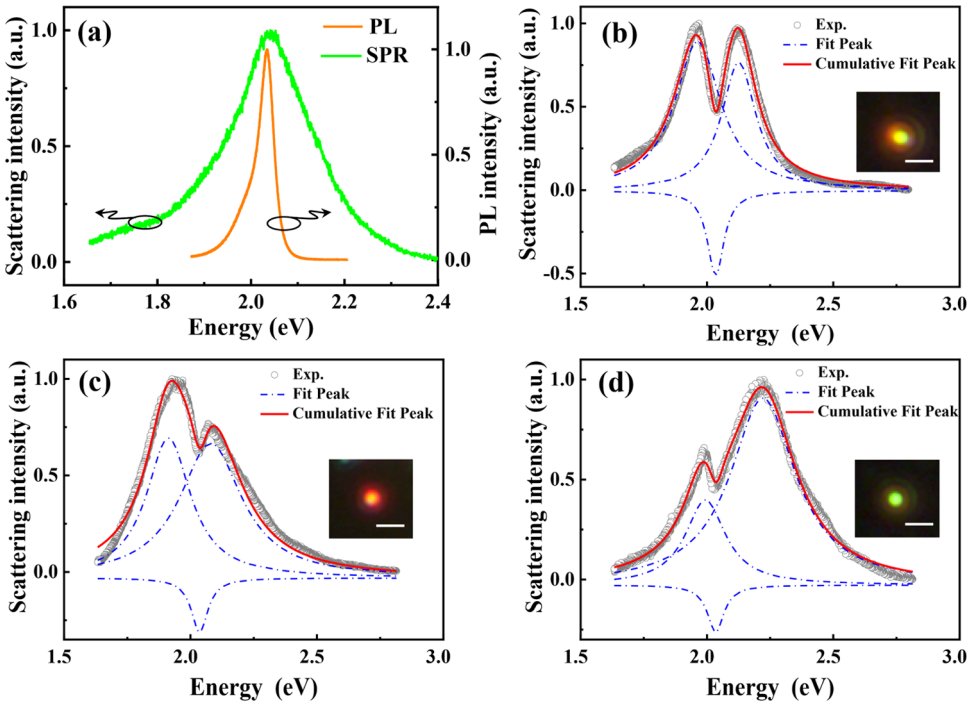

Figure 2. (a) PL spectrum of monolayer WS_2 (orange curve) and scattering spectrum of a plasmonic nanocavity (green curve) in air. (b, c, d) DF scattering spectra of three representative WS_2-Ag nanocavities with different colors. Inset: DF scattering image. Scale bars are 1 μm. Gray dots show the measured scattering response. Blue dashed lines show the individual Lorentzian fits and red solid lines show the combined fits.

(DCM) and ethanol. By increasing the concentration of DCM, the RS energy is tuned from 183 meV (in ethanol) to 273 meV (in DCM) continuously, which is mainly attributed to the remarkable increase of the neutral exciton density in monolayer WS_2 as the concentration of DCM is increased. To the best of our knowledge, it shows the largest RS energy value up to 273 meV with a tuning width of 90 meV in layered TMDCs/plasmonic nanocavity. In addition, this method is a very simple and convenient technique with high reversibility. It may have potential applications in quantum information processing and manipulating chemical reactions.

2. RESULTS AND DISCUSSION

2.1. Sample Characterization. The schematic diagram of the WS_2-Ag nanocavity is shown in the inset of Figure 1a. The

https://doi.org/10.1021/acsami.1c10295
ACS Appl. Mater. Interfaces XXXX, XXX, XXX−XXX

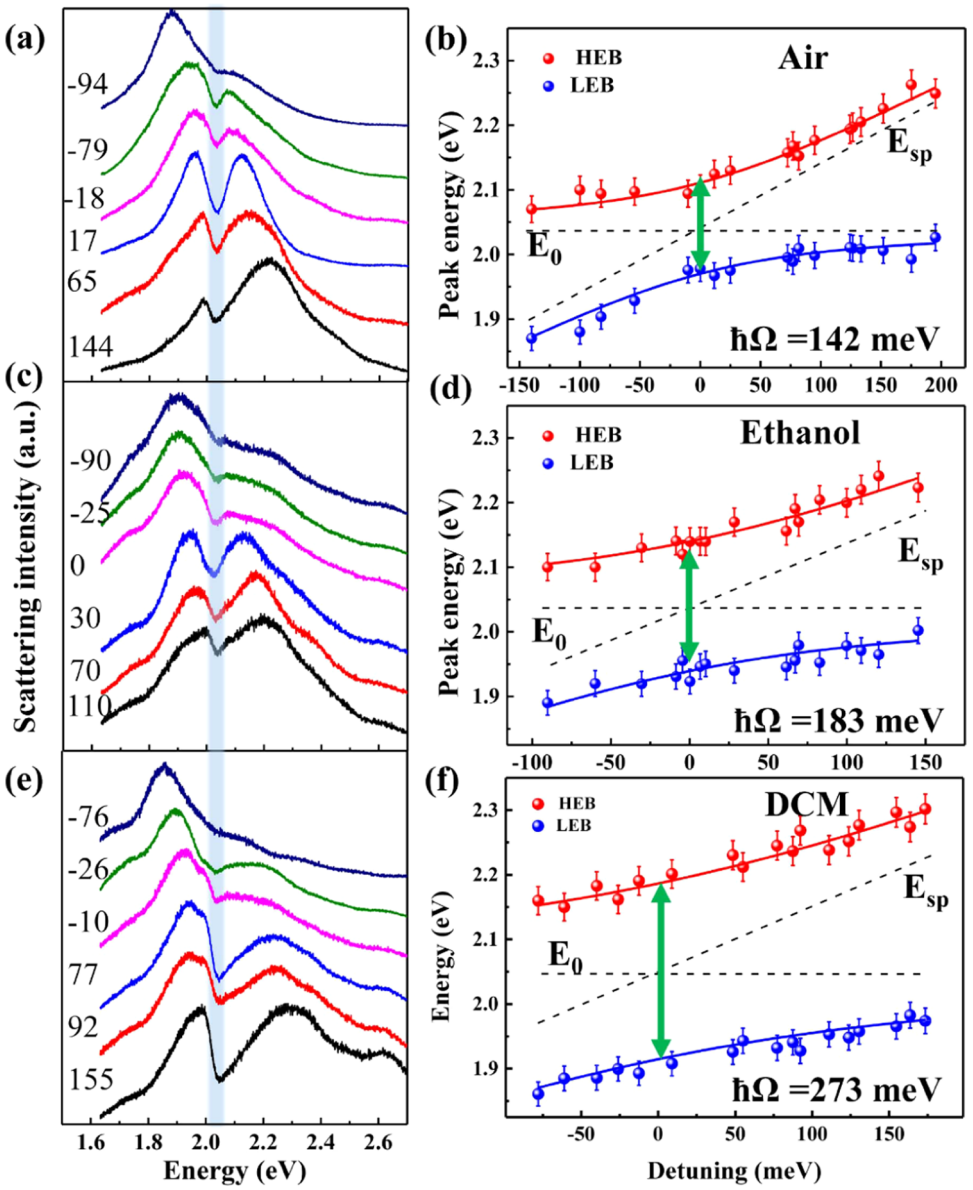

Figure 3. (a, c, e) Scattering spectra from hybrids with different sizes of Ag nanocubes in air, ethanol, and DCM, respectively. The detuning energy (meV) of each spectrum is listed on the left. The blue band marks the neutral exciton position in the bare WS_2 monolayer. (b, d, f) Dispersions of the hybrid states in air, ethanol, and DCM, respectively. It is extracted from the experimental data (red and blue dots) and calculated using eq 1 (red and blue lines). The black dashed lines represent the uncoupled exciton transition energy and plasmon resonance energy.

plasmonic nanocavity belongs to a highly confined nanoparticle over mirror (NPoM) geometry, which consists of a single Ag nanocube and an Ag film. The surface plasmon resonance (SPR) of the plasmonic nanocavity can be tuned by the nanogap thickness and nanocube size. A 9 nm thick spacer film (Al_2O_3) and monolayer WS_2 were inserted into the nanogap. The dark-field (DF) scattering spectra and photoluminescence (PL) spectra of single hybrids were measured with an optical microscope (Olympus, BX 53), as schematically shown in Figure 1a. Figure 1b shows an optical image of the WS_2-Ag nanocavity. The dark yellow area presents a WS_2 flake and red dots present single Ag nanocubes. The transmission electron microscopy (TEM) image in the inset shows a Ag nanocube with an edge length of ~75 nm. The corresponding DF scattering image is shown in Figure 1c. The white dashed curve indicates the edges of WS_2 and the bright spots present single nanocubes. Different colors correspond to the Ag nanocubes with varied sizes, indicating the resonant position of the nanocavity. In Figure 1d, the atomic force microscopy (AFM) image shows a triangular WS_2 flake. The height profile (inset) indicates that monolayer WS_2 with a thickness of ~0.7 nm is used. Figure 1e shows the absorption of monolayer WS_2 on the sapphire, displaying three peaks corresponding to neutral A-, B-, and C-excitons. A-exciton is fitted by a Lorentzian shape with parameters: E_0 = 2.036 eV and γ = 0.08 eV.

The orange curve shown in Figure 2a is the PL spectrum of monolayer WS_2. The green curve is the scattering spectrum of the plasmonic nanocavity in air, which is tuned to overlap the PL peak by adjusting the thickness of the Al_2O_3 film. The quality factor, Q, of the nanocavity in air is calculated to be ~10. Then, the scattering spectra of the hybrids with different colors shown in Figure 1c are measured. Three representative scattering spectra of yellow, red, and green spots are shown in

https://doi.org/10.1021/acsami.1c10295
ACS Appl. Mater. Interfaces XXXX, XXX, XXX−XXX

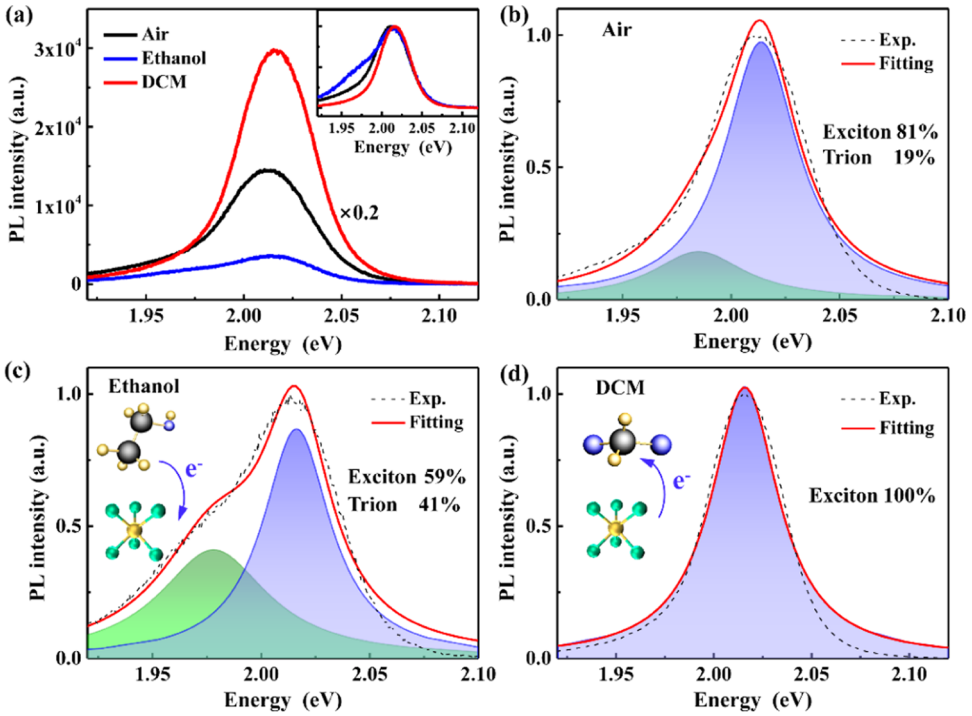

Figure 4. (a) PL spectra of monolayer WS_2 on an Al_2O_3−Ag film. Inset: normalized PL spectra. (b−d) PL spectra of pristine and solvent-immersed WS_2 (dashed black) deconvoluted into the exciton (~615 nm; purple area) and trion (~626 nm; green area) peaks. The convoluted PL spectra are shown in red. The spectral weights of the exciton and trion peaks are (b) 81 and 19%, (c) 59 and 41%, and (d) nearly 100% exciton, respectively. Insets of (b and c): artist view on electron transfer between WS_2 and solvents.

Figure 2b−d, respectively. Clearly, the scattering spectra reveal the resonance mode splitting. It arises from strong plasmon−exciton coupling, that is, the formation of plexcitons, as will be demonstrated later. It is worth noting that the WS_2 monolayer has large values for the real and imaginary parts of its dielectric permittivity (absorption coefficient: $\alpha = 3.6 \times 10^5$ cm^{-1}).[26] Thus, exciton absorption has an important influence on the scattering spectra of hybrids. For fitting the scattering spectra, a three-Lorentzian model is developed. As shown in Figure 2b−d, each blue dashed line shows the individual Lorentzian shape fit. Specifically, the fitting of the positive amplitude is used to fit the two peaks, and the negative amplitude is added by taking into account the effect of the exciton absorption of the WS_2 monolayer. During fitting, the Lorentz parameters of the negative amplitude come from the absorption spectrum shown in Figure 1e (see the Supporting Information (SI) for the fitting details). It can be seen that the numerical fittings (red curves) are in good agreement with the experimental data (gray dots).

2.2. Enhancement of Coupling Strength in Solvents.

Figure 3a presents the scattering spectra of the WS_2-Ag nanocavity with different Ag nanocube sizes in air (see Figure S1 in the SI). It is observed that the mode splittings are shifted at different detuning energies. The energy peaks higher (or lower) than the exciton energy are defined as the high (or low) energy branch (HEB or LEB). The values of HEB and LEB are extracted from the scattering spectra by fitting with the three-Lorentzian model. Then, the energy peaks as a function of detuning can be traced out, showing an anticrossing curve in Figure 3b. It can be fitted with the semiclassical coupled oscillator model (SCCOM)

$$E_{\pm} = \frac{1}{2}(E_{SP} + E_0 \pm \sqrt{4g^2 + \delta^2}) \quad (1)$$

where $E_{\pm}$ are the eigen energies of the hybrid system, $\delta = E_{SP} - E_0$ is the detuning energy between uncoupled surface plasmon energy (E_{sp}) and neutral exciton energy (E_0), E_{sp} is obtained by $E_{SP} = E_+ + E_- - E_0$, and g is the coupling strength. The two hybrid states exhibit plasmon−exciton dispersion characteristics with an RS energy of $\hbar\Omega = 2g = 142$ meV, at $E_{sp} = E_0$. Figure 3c,e presents the measured multiple scattering spectra in ethanol and DCM, respectively, and extracted anticrossing curves are shown in Figure 3d,f, respectively. Specifically, the weak scattering peaks at ~1.8 and ~2.6 eV are originated from the Al_2O_3/Ag/Si substrate and the edge of the WS_2 monolayer, respectively (see the SI for details). The RS energies are calculated to be 183 and 273 meV for ethanol- and DCM-immersed hybrid systems, respectively. Obviously, the coupling strengths in solvent-immersed hybrids are both enhanced in comparison to that in air. It is worth noting that the line widths of the exciton and the surface plasmon (in air), γ_0 and γ_{sp}, are extracted to be ~50 and ~214 meV from Figure 2a. In addition, the line widths of the surface plasmon, γ_{sp}, in ethanol and in DCM are extracted as ~238 and ~263 meV (see Figure S2 in the SI). The polariton line widths, $\frac{\gamma_{SP}+\gamma_0}{2}$, are calculated to be 132 meV (in air), 144 meV (in ethanol), and 156 meV (in DCM). Therefore, the strong coupling is achieved in our experiment because the polariton line widths are smaller than the corresponding RS energies.[27−29]

For analyzing the enhancement mechanism of coupling strength in different solvents, we first study the solvent effect on the PL property from monolayer WS_2. Figure 4a shows the PL spectra of WS_2 in air or immersed in different solvents under excitation of a continuous-wave laser at 473 nm. In

https://doi.org/10.1021/acsami.1c10295
ACS Appl. Mater. Interfaces XXXX, XXX, XXX−XXX

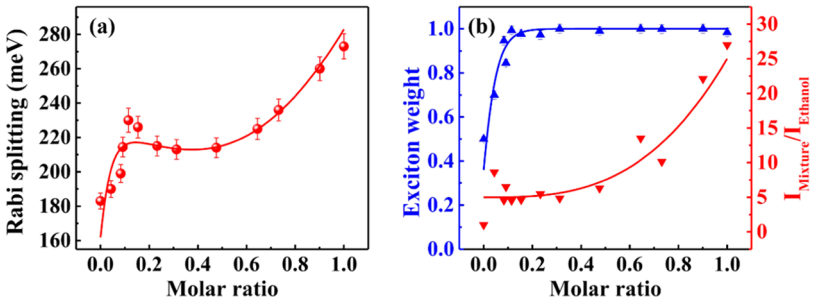

Figure 5. (a) RS energy in a WS_2-Ag nanocavity as a function of molar ratio. (b) Measured exciton weight (blue dots) and the relative PL intensity (red dot) in monolayer WS_2 as a function of molar ratio. The blue and red curves indicate the numerical fitting results.

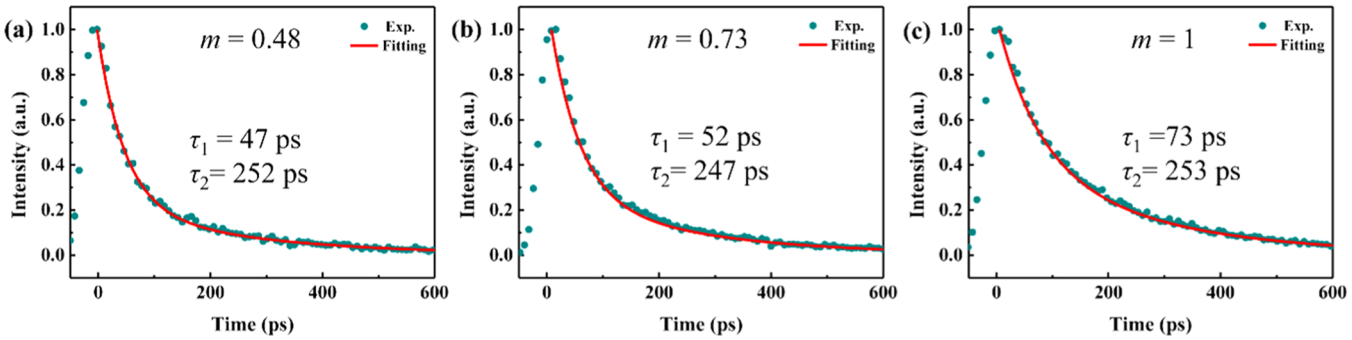

Figure 6. (a–c) PL decay results (green dots) for bare WS_2 on the Al_2O_3/Ag film in DCM/ethanol mixed solvents with molar ratios of 0.48, 0.73, and 1.0, respectively. The red curves indicate the fitted results with a biexponential decay function.

general, it is observed that PL intensities are enhanced and quenched in DCM and ethanol solvents compared to that in air, respectively. The inset shows the normalized PL spectra at the same peak position with quite different spectral profiles. Specifically, an extra peak is observed in ethanol-immersed WS_2. In Figure 4b,c, the spectra are analyzed by deconvoluting into two Lorentzian profiles of the exciton (X at ∼615 nm) and trion (X^- at ∼626 nm) peaks.[30] The spectral weights of the exciton and the trion in monolayer WS_2 in air (Figure 4b) are fitted to be 81 and 19%, respectively. The trion emission originates from the transition of two electrons bound to one hole, on account of abundant electrons in n-type WS_2.[23] In ethanol-immersed WS_2 (Figure 4c), the exciton weight is decreased to 59%, the trion weight is increased to 41%. In contrast, DCM-immersed WS_2 (Figure 4d) displays the opposite behavior. The fitting result shows that only the neutral exciton spectrum is observed (∼100%). The variation of the exciton/trion ratio in solvent-immersed WS_2 is attributed to the electron transfer between solvents and WS_2.[24]

For any two interacting molecules, the difference in electronegativity drives electron transfer and determines the electron flow direction. Electronegativity (χ) characterizes the ability of an atom to attract electrons in a material, which is defined as[31]

$$\chi = \frac{1}{2}\mathrm{IP} + \mathrm{EA} \tag{2}$$

where IP is the ionization potential and EA is the electron affinity. Thus, the electronegativity value of ethanol and DCM are calculated to be 2.49 and 5.05 eV, respectively.[31−34] The electronegativity of TMDCs can be expressed as[35,36]

$$\chi_{\mathrm{TMDC}} = E_{\mathrm{VBM}} + E_{\mathrm{e}} - 0.55E_{\mathrm{g}} \tag{3}$$

where E_{VBM} is the potential of the valence band maximum (VBM) against a normal hydrogen electrode (NHE), E_{e} is the standard electrode potential on the NHE scale, and E_{g} is the band gap. The electronegativity value of monolayer WS_2 is calculated to be ∼4.83 eV,[37,38] which is smaller than that of DCM. Therefore, monolayer WS_2 loses residual electrons in the DCM solvent, and the spectral weight of the exciton is increased up to nearly 100%. On the contrary, monolayer WS_2 in ethanol attracts electrons, and the exciton weight is decreased to 59%. In the experiment, the exciton weight in DCM-immersed WS_2 is increased by ∼1.2 times, while in ethanol-immersed one, it is decreased by ∼0.7 times. Therefore, it inspires us to control the coupling strength by tuning the exciton number in a mixed solution of DCM/ethanol.

2.3. Continuous Tuning of Coupling Strength. Figure 5a exhibits the RS energy as a function of molar ratio. The molar ratio is defined as the mole fraction of DCM in a mixed solution of DCM/ethanol, denoted *m*. Figure 5b shows the exciton weight (blue dots) and relative PL intensity (red dots) averaged in several monolayer WS_2. As the molar ratio is increased from 0 to 0.12, the proportion of neutral excitons in the monolayer WS_2 is increased from 50 to 95%, and the measured RS energy is increased rapidly from 183 to 230 meV accordingly. Therefore, the increased exciton number due to electron transfer is the dominating reason for the coupling enhancement in the molar ratio (0−0.12). As the molar ratio is further increased (0.12−0.4), the measured RS energy shows a slight decrease to 210 meV. Since the exciton weight and the PL intensity show a small variation, the decrease of RS energy may be attributed to the fact that the transition dipole moment of DCM is smaller than that of ethanol. As the molar ratio is increased from 0.4 to 1.0, the measured RS energy is increased from 210 to 273 meV. Figure 5b shows that the PL intensity is

https://doi.org/10.1021/acsami.1c10295
ACS Appl. Mater. Interfaces XXXX, XXX, XXX−XXX

increased, while the exciton weight is stable, implying that the enhanced PL intensity is not due to charge transfer. Furthermore, the PL lifetime of monolayer WS_2 in the mixed solution at different molar ratios is shown in Figure 6. The red curves show the numerical fittings with a biexponential decay function, which consists of a fast component (τ_1) and a slow component (τ_2). As the molar ratio is increased from 0.48 to 1, τ_1 is increased from 47 to 73 ps, while τ_2 keeps a constant of ~250 ps. Generally, the fast component represents the nonradiative recombination related to the defect states. The increased τ_1 indicates that the defects in WS_2 are repaired by DCM.[39] Thus, the exciton number in the molar ratio (0.4−1.0) is significantly increased.

Following is the detailed analysis of RS energy tuning. The coupling strength between the exciton and the surface plasmon is given by[27,40,41]

$$g = \mu\sqrt{\frac{4\pi h_{bar} Nc}{\lambda \varepsilon \varepsilon_0 V}} \propto \mu\sqrt{N/V} \tag{4}$$

where μ is the exciton transition dipole moment of monolayer WS_2,[9] N and λ are the number and wavelength of the exciton, ε is the dielectric function, and V is the effective mode volume of the nanocavity. According to the definition of the effective mode volume of the optical cavity,[42] the mode volume of the Ag nanocavity is calculated to be around $V = 0.001(\lambda/n)^3$,[43] where n is the effective refractive index in the nanocavity. Since the nanogap is surrounded by the solvent, Al_2O_3, and poly(vinylpyrrolidone) (PVP), the value of n can be calculated by $n \approx (n_{solvent} + n_{Al_2O_3} + n_{PVP})/3$. The refractive indices of ethanol and DCM are 1.36 and 1.42, respectively. Thus, the refractive index of the plasmonic nanocavity is calculated to be 1.42 in air, 1.54 in ethanol, and 1.56 in DCM. The mode volume is 82×10^3 nm^3 in air, 64×10^3 nm^3 in ethanol, and 62×10^3 nm^3 in DCM. Since the refractive index of the nanocavity shows a low variation of 1.3% in ethanol/DCM, V can be regarded as a constant for calculating the coupling strength.

According to static screening approximation, the relative exciton transition dipole moment of TMDCs in solvents can be estimated by $\mu_{solvent}/\mu_{air} \approx \sqrt{\varepsilon_{eff}}$,[44] where ε_{eff} is the effective dielectric constant. ε_{eff} of the monolayer WS_2-Ag nanocavity can be estimated as $\varepsilon_{eff} \approx (\varepsilon_{solvent} + \varepsilon_{Al_2O_3} + \varepsilon_{PVP})/3$, where $\varepsilon_{solvent}$ is the static dielectric constant of the solvent. $\varepsilon_{Al_2O_3} = 4.5$ and $\varepsilon_{PVP} = 2.37$ are the dielectric constants of Al_2O_3 and PVP, respectively. The static dielectric constants of ethanol and DCM are 25.3 and 8.93, respectively. For the hybrid in ethanol and DCM, it is obtained that $\mu_{ethanol}/\mu_{air} = 2.02$ and $\mu_{DCM}/\mu_{air} = 1.41$, respectively. Thus, the relative $\mu(m)$ as a function of molar ratio is written as

$$\mu(m) = m\mu_{DCM}/\mu_{air} + (1 - m)\mu_{ethanol}/\mu_{air} = 2.02 - 0.61m \tag{5}$$

For calculating the exciton number, both the exciton weight and PL intensity in the mixed solvent are considered. In Figure 5b, the exciton weight $W(m)$ and the relative PL intensity $I(m)$ as a function of the molar ratio of DCM/ethanol are numerically fitted by

$$W(m) = (1 - 0.4e^{-25m})^2 \tag{6}$$

$$I(m) = 5 + 20m^3 \tag{7}$$

PL intensity is proportional to the square of the exciton transition dipole moment and is also proportional to the exciton number. The exciton number (N) (Figure S3) in monolayer WS_2 can be calculated by

$$N(m) = N_0 W(m) + I(m)/\mu^2(m) \tag{8}$$

where N_0 is the intrinsic exciton number of monolayer WS_2. According to eqs 4, 5, and 8, the RS energy can be fitted as shown in Figure 5a (red curve), which is in good agreement with the experimental data. It indicates that the tuning of coupling strength in solvents is mainly ascribed to the electron transfer and defect passivation, as well as the variation of the transition dipole moment. In addition, the calculated scattering spectra in air, ethanol, and DCM are shown in Figure S8 by Comsol Multiphysics. By tuning the oscillator strength value of monolayer WS_2, a similar RS energy is obtained. We thus conclude that changing the dielectric environment of a coupled plasmon−exciton system comprising an Ag nanocube and monolayer WS_2 is very useful for tuning the coupling strength.

3. CONCLUSIONS

In summary, we demonstrate active exciton manipulation of plexcitonic coupling in a monolayer WS_2-Ag nanocavity by immersing in a mixed DCM/ethanol solution. An RS energy up to 273 meV is obtained by immersing in the DCM solvent, which is, to the best of our knowledge, the largest value reported for the layered TMDCs/plasmonic nanocavity. More importantly, the RS energy can be tuned from 142 meV (in air) to 273 meV (in DCM) by adjusting the solvent with different mixture ratios, indicating a large tuning width of 131 meV. It is mainly attributed to the remarkable increase of the neutral exciton density in monolayer WS_2 as the concentration of DCM is increased. This method is very simple and convenient with high reversibility. Thus, it may open a new avenue within the area of engineering strong coupling with enhanced coupling strength in the layered TMDCs/plasmonic cavity, which has potential applications in quantum information processing and nonlinear optical materials.

4. METHODS

4.1. Sample Preparation. The plasmonic nanocavity was fabricated with a self-assembly method. First, a Ti/Ag thin film with a thickness of ~10/80 nm was coated on silicon wafers using electron beam evaporation. Then, the Al_2O_3 spacer film was deposited on the Ag-coated substrate by atomic layer deposition (ALD) at 100 °C. WS_2 flakes (Sixcarbon Tech. Shenzhen) were grown on sapphires by the chemical vapor deposition (CVD) method. To avoid introducing dust, we transferred WS_2 flakes from the sapphire to the Al_2O_3−Ag film with polydimethylsiloxane (PDMS).[45] Finally, the Ag nanocubes with a PVP layer (nanoComposix, size of 65−95 nm) were drop-coated onto the WS_2 monolayer and were rinsed off with deionized water to remove excess nanocubes. The sample was then blow-dried using nitrogen gas. Ag nanocubes were monodispersed on the Al_2O_3−Ag film uniformly. To avoid coupling among Ag nanocubes, a proper distribution of nanocubes is necessary. For preparing the solvent-immersed hybrids, about 10 μL of the solution was dropped on the sample, forming a thin film with a thickness of ~100 μm under a coverslip. The sample surfaces were cleaned with pure ethanol before changing the solvent. Typically, it takes about 1 min to clean and prepare samples. All experiments were performed at room temperature.

4.2. Optical Measurements. For DF scattering measurements, the sample was illuminated by a 100-W halogen lamp through a BD objective (Olympus, 100×, NA = 0.9, MPLFL N). Scattered light was collected by the same objective and focused by a lens. A pinhole (100

https://doi.org/10.1021/acsami.1c10295
ACS Appl. Mater. Interfaces XXXX, XXX, XXX−XXX

μm) was placed on the focus plane to select a specific nanoparticle. The scattered signal was focused by another lens and analyzed with a CCD (Qimaging, QICAM B series) or a spectrometer (Andor, SR303i). PL signals were excited by a continuous laser at 473 nm and detected by a spectrometer. Time-resolved PL measurements were performed using a 400 nm pulsed laser (Coherent, Ti:sapphire, a repetition rate of 80 MHz). The laser was focused by a 20× objective (Olympus, NA = 0.4) at an excitation power of ~1 kW cm^{-2}. The PL signal was detected using a time-corrected single-photon counting module (Pico-Harp 300, PicoQuant, detector: PD-100-CTC). All of the experiments were performed at room temperature.

■ ASSOCIATED CONTENT

Supporting Information

The Supporting Information is available free of charge at https://pubs.acs.org/doi/10.1021/acsami.1c10295.

Scattering spectra of different sizes of Ag nanocubes and nanocavity in solvents; calculation of the exciton number; fitting of the scattering spectra; and simulation of the scattering spectra (PDF)

■ AUTHOR INFORMATION

Corresponding Authors

Kai Wang − *Wuhan National Laboratory for Optoelectronics and School of Physics, Huazhong University of Science and Technology, Wuhan 430074, China*; Email: kale_wong@hust.edu.cn

Peixiang Lu − *Hubei Key Laboratory of Optical Information and Pattern Recognition, Wuhan Institute of Technology, Wuhan 430205, China; Wuhan National Laboratory for Optoelectronics and School of Physics, Huazhong University of Science and Technology, Wuhan 430074, China; Guangdong Intelligent Robotics Institute, Dongguan 523808, China*; Email: lupeixiang@hust.edu.cn

Authors

Xiaobo Han − *Hubei Key Laboratory of Optical Information and Pattern Recognition, Wuhan Institute of Technology, Wuhan 430205, China*

Yanan Jiang − *Wuhan National Laboratory for Optoelectronics and School of Physics, Huazhong University of Science and Technology, Wuhan 430074, China*

Xiangyuan Xing − *Wuhan National Laboratory for Optoelectronics and School of Physics, Huazhong University of Science and Technology, Wuhan 430074, China*

Shujin Li − *Wuhan National Laboratory for Optoelectronics and School of Physics, Huazhong University of Science and Technology, Wuhan 430074, China*

Huatian Hu − *Hubei Key Laboratory of Optical Information and Pattern Recognition, Wuhan Institute of Technology, Wuhan 430205, China*

Weiwei Liu − *Wuhan National Laboratory for Optoelectronics and School of Physics, Huazhong University of Science and Technology, Wuhan 430074, China*; orcid.org/0000-0001-9451-1968

Bing Wang − *Wuhan National Laboratory for Optoelectronics and School of Physics, Huazhong University of Science and Technology, Wuhan 430074, China*

Complete contact information is available at: https://pubs.acs.org/10.1021/acsami.1c10295

Notes

The authors declare no competing financial interest.

■ ACKNOWLEDGMENTS

This work was supported by the Basic and Applied Basic Research Major Program of Guangdong Province (No. 2019B030302003) and the National Natural Science Foundation of China (Nos 11904271, 11774115, 91850113, and 12021004). The authors thank Prof. Jun Zhou for Al_2O_3 film fabrication. Special thanks to the Analytical and Testing Center of HUST and the Center for Nanoscale Characterization & Devices (CNCD) of WNLO for using their facilities.

■ REFERENCES

(1) Törmä, P.; Barnes, W. L. Strong Coupling between Surface Plasmon Polaritons and Emitters: A Review. *Rep. Prog. Phys.* **2015**, *78*, No. 013901.

(2) Piccione, B.; Aspetti, C. O.; Cho, C.-H.; Agarwal, R. Tailoring Light−Matter Coupling in Semiconductor and Hybrid-Plasmonic Nanowires. *Rep. Prog. Phys.* **2014**, *77*, No. 086401.

(3) Liu, X.; Bao, W.; Li, Q.; Ropp, C.; Wang, Y.; Zhang, X. Control of Coherently Coupled Exciton Polaritons in Monolayer Tungsten Disulphide. *Phys. Rev. Lett.* **2017**, *119*, No. 027403.

(4) Sugawara, Y.; Kelf, T. A.; Baumberg, J. J.; Abdelsalam, M. E.; Bartlett, P. N. Strong Coupling between Localized Plasmons and Organic Excitons in Metal Nanovoids. *Phys. Rev. Lett.* **2006**, *97*, No. 266808.

(5) Schwartz, T.; Hutchison, J. A.; Genet, C.; Ebbesen, T. W. Reversible Switching of Ultrastrong Light-Molecule Coupling. *Phys. Rev. Lett.* **2011**, *106*, No. 196405.

(6) Bellessa, J.; Bonnand, C.; Plenet, J. C.; Mugnier, J. Strong Coupling between Surface Plasmons and Excitons in an Organic Semiconductor. *Phys. Rev. Lett.* **2004**, *93*, No. 036404.

(7) Tserkezis, C.; Fernandez-Dominguez, A. I.; Goncalves, P. A. D.; Todisco, F.; Cox, J. D.; Busch, K.; Stenger, N.; Bozhevolnyi, S. I.; Mortensen, N. A.; Wolff, C. On the Applicability of Quantum-Optical Concepts in Strong-Coupling Nanophotonics. *Rep. Prog. Phys.* **2020**, *83*, No. 082401.

(8) Schneider, C.; Glazov, M. M.; Korn, T.; Hofling, S.; Urbaszek, B. Two-Dimensional Semiconductors in the Regime of Strong Light-Matter Coupling. *Nat. Commun.* **2018**, *9*, No. 2695.

(9) Wen, J.; Wang, H.; Wang, W.; Deng, Z.; Zhuang, C.; Zhang, Y.; Liu, F.; She, J.; Chen, J.; Chen, H.; Deng, S.; Xu, N. Room-Temperature Strong Light-Matter Interaction with Active Control in Single Plasmonic Nanorod Coupled with Two-Dimensional Atomic Crystals. *Nano Lett.* **2017**, *17*, 4689−4697.

(10) Zheng, D.; Zhang, S.; Deng, Q.; Kang, M.; Nordlander, P.; Xu, H. Manipulating Coherent Plasmon-Exciton Interaction in a Single Silver Nanorod on Monolayer WSe_2. *Nano Lett.* **2017**, *17*, 3809−3814.

(11) Sun, J.; Hu, H.; Zheng, D.; Zhang, D.; Deng, Q.; Zhang, S.; Xu, H. Light-Emitting Plexciton: Exploiting Plasmon-Exciton Interaction in the Intermediate Coupling Regime. *ACS Nano* **2018**, *12*, 10393−10402.

(12) Yankovich, A. B.; Munkhbat, B.; Baranov, D. G.; Cuadra, J.; Olsen, E.; Lourenco-Martins, H.; Tizei, L. H. G.; Kociak, M.; Olsson, E.; Shegai, T. Visualizing Spatial Variations of Plasmon-Exciton Polaritons at the Nanoscale Using Electron Microscopy. *Nano Lett.* **2019**, *19*, 8171−8181.

(13) Wang, S.; Li, S.; Chervy, T.; Shalabney, A.; Azzini, S.; Orgiu, E.; Hutchison, J. A.; Genet, C.; Samori, P.; Ebbesen, T. W. Coherent Coupling of WS_2 Monolayers with Metallic Photonic Nanostructures at Room Temperature. *Nano Lett.* **2016**, *16*, 4368−74.

(14) Stührenberg, M.; Munkhbat, B.; Baranov, D. G.; Cuadra, J.; Yankovich, A. B.; Antosiewicz, T. J.; Olsson, E.; Shegai, T. Strong Light-Matter Coupling between Plasmons in Individual Gold Bi-Pyramids and Excitons in Mono- and Multilayer WSe_2. *Nano Lett.* **2018**, *18*, 5938−5945.

(15) Han, X.; Wang, K.; Xing, X.; Wang, M.; Lu, P. Rabi Splitting in a Plasmonic Nanocavity Coupled to a WS2 Monolayer at Room Temperature. *ACS Photonics* **2018**, *5*, 3970−3976.
(16) Qin, J.; Chen, Y. H.; Zhang, Z.; Zhang, Y.; Blaikie, R. J.; Ding, B.; Qiu, M. Revealing Strong Plasmon-Exciton Coupling between Nanogap Resonators and Two-Dimensional Semiconductors at Ambient Conditions. *Phys. Rev. Lett.* **2020**, *124*, No. 063902.
(17) Geisler, M.; Cui, X. M.; Wang, J. F.; Rindzevicius, T.; Gammelgaard, L.; Jessen, B. S.; Goncalves, P. A. D.; Todisco, F.; Boggild, P.; Boisen, A.; Wubs, M.; Mortensen, N. A.; Xiao, S. S.; Stenger, N. Single-Crystalline Gold Nanodisks on WS_2 Mono- and Multilayers for Strong Coupling at Room Temperature. *ACS Photonics* **2019**, *6*, 994−1001.
(18) Wersäll, M.; Cuadra, J.; Antosiewicz, T. J.; Balci, S.; Shegai, T. Observation of Mode Splitting in Photoluminescence of Individual Plasmonic Nanoparticles Strongly Coupled to Molecular Excitons. *Nano Lett.* **2017**, *17*, 551−558.
(19) Schlather, A. E.; Large, N.; Urban, A. S.; Nordlander, P.; Halas, N. J. Near-Field Mediated Plexcitonic Coupling and Giant Rabi Splitting in Individual Metallic Dimers. *Nano Lett.* **2013**, *13*, 3281−3286.
(20) Moilanen, A. J.; Hakala, T. K.; Törmä, P. Active Control of Surface Plasmon−Emitter Strong Coupling. *ACS Photonics* **2018**, *5*, 54−64.
(21) Lee, B.; Liu, W.; Naylor, C. H.; Park, J.; Malek, S. C.; Berger, J. S.; Johnson, A. T. C.; Agarwal, R. Electrical Tuning of Exciton-Plasmon Polariton Coupling in Monolayer MoS_2 Integrated with Plasmonic Nanoantenna Lattice. *Nano Lett.* **2017**, *17*, 4541−4547.
(22) Chakraborty, B.; Gu, J.; Sun, Z.; Khatoniar, M.; Bushati, R.; Boehmke, A. L.; Koots, R.; Menon, V. M. Control of Strong Light-Matter Interaction in Monolayer WS_2 through Electric Field Gating. *Nano Lett.* **2018**, *18*, 6455−6460.
(23) Peimyoo, N.; Yang, W.; Shang, J.; Shen, X.; Wang, Y.; Yu, T. Chemically Driven Tunable Light Emission of Charged and Neutral Excitons in Monolayer WS_2. *ACS Nano* **2014**, *8*, 11320−11329.
(24) Choi, J.; Zhang, H.; Du, H.; Choi, J. H. Understanding Solvent Effects on the Properties of Two-Dimensional Transition Metal Dichalcogenides. *ACS Appl. Mater. Interfaces* **2016**, *8*, 8864−9.
(25) Lin, Y.; Ling, X.; Yu, L.; Huang, S.; Hsu, A. L.; Lee, Y. H.; Kong, J.; Dresselhaus, M. S.; Palacios, T. Dielectric Screening of Excitons and Trions in Single-Layer MoS_2. *Nano Lett.* **2014**, *14*, 5569−5576.
(26) Jung, G.-H.; Yoo, S.; Park, Q. H. Measuring the Optical Permittivity of Two-Dimensional Materials without a Priori Knowledge of Electronic Transitions. *Nanophotonics* **2018**, *8*, 263−270.
(27) Zengin, G.; Wersall, M.; Nilsson, S.; Antosiewicz, T. J.; Kall, M.; Shegai, T. Realizing Strong Light-Matter Interactions between Single-Nanoparticle Plasmons and Molecular Excitons at Ambient Conditions. *Phys. Rev. Lett.* **2015**, *114*, No. 157401.
(28) Khitrova, G.; Gibbs, H. M.; Kira, M.; Koch, S. W.; Scherer, A. Vacuum Rabi Splitting in Semiconductors. *Nat. Phys.* **2006**, *2*, 81−90.
(29) Pelton, M.; Storm, S. D.; Leng, H. Strong Coupling of Emitters to Single Plasmonic Nanoparticles: Exciton-Induced Transparency and Rabi Splitting. *Nanoscale* **2019**, *11*, 14540−14552.
(30) Plechinger, G.; Nagler, P.; Kraus, J.; Paradiso, N.; Strunk, C.; Schuller, C.; Korn, T. Identification of Excitons, Trions and Biexcitons in Single-Layer WS_2. *Phys. Status Solidi RRL* **2015**, *9*, 457−461.
(31) Pearson, R. G. Absolute Electronegativity and Hardness: Application to Inorganic Chemistry. *Inorg. Chem.* **1988**, *27*, 734−740.
(32) Linstrom, P. J.; Mallard, W. G. The Nist Chemistry Webbook: A Chemical Data Resource on the Internet. *J. Chem. Eng. Data* **2001**, *46*, 1059−1063.
(33) Santhanam, K. S. V.; Sangoi, R.; Fuller, L. A Chemical Sensor for Chloromethanes Using a Nanocomposite of Multiwalled Carbon Nanotubes with Poly(3-Methylthiophene). *Sens. Actuators, B* **2005**, *106*, 766−771.
(34) Nist Computational Chemistry Comparison and Benchmark Database, Http://Cccbdb.Nist.Gov/, the Humo and Lumo of Ethanol Are Calculated Using the B3lyp Method with 6-31g** Basis Set.
(35) Amin, B.; Singh, N.; Schwingenschlogl, U. Heterostructures of Transition Metal Dichalcogenides. *Phys. Rev. B* **2015**, *92*, No. 075439.
(36) Singh, N.; Jabbour, G.; Schwingenschlogl, U. Optical and Photocatalytic Properties of Two-Dimensional MoS_2. *Eur. Phys. J. B* **2012**, *85*, No. 392.
(37) Gong, C.; Zhang, H. J.; Wang, W. H.; Colombo, L.; Wallace, R. M.; Cho, K. J. Band Alignment of Two-Dimensional Transition Metal Dichalcogenides: Application in Tunnel Field Effect Transistors. *Appl. Phys. Lett.* **2013**, *103*, No. 053513.
(38) Kang, J.; Tongay, S.; Zhou, J.; Li, J.; Wu, J. Band Offsets and Heterostructures of Two-Dimensional Semiconductors. *Appl. Phys. Lett.* **2013**, *102*, No. 012111.
(39) Tanoh, A. O. A.; Alexander-Webber, J.; Xiao, J.; Delport, G.; Williams, C. A.; Bretscher, H.; Gauriot, N.; Allardice, J.; Pandya, R.; Fan, Y.; Li, Z.; Vignolini, S.; Stranks, S. D.; Hofmann, S.; Rao, A. Enhancing Photoluminescence and Mobilities in WS_2 Monolayers with Oleic Acid Ligands. *Nano Lett.* **2019**, *19*, 6299−6307.
(40) Chikkaraddy, R.; de Nijs, B.; Benz, F.; Barrow, S. J.; Scherman, O. A.; Rosta, E.; Demetriadou, A.; Fox, P.; Hess, O.; Baumberg, J. J. Single-Molecule Strong Coupling at Room Temperature in Plasmonic Nanocavities. *Nature* **2016**, *535*, 127−130.
(41) Cuadra, J.; Baranov, D. G.; Wersall, M.; Verre, R.; Antosiewicz, T. J.; Shegai, T. Observation of Tunable Charged Exciton Polaritons in Hybrid Monolayer WS_2-Plasmonic Nanoantenna System. *Nano Lett.* **2018**, *18*, 1777−1785.
(42) Huang, S.; Ming, T.; Lin, Y.; Ling, X.; Ruan, Q.; Palacios, T.; Wang, J.; Dresselhaus, M.; Kong, J. Ultrasmall Mode Volumes in Plasmonic Cavities of Nanoparticle-on-Mirror Structures. *Small* **2016**, *12*, 5190−5199.
(43) Akselrod, G. M.; Ming, T.; Argyropoulos, C.; Hoang, T. B.; Lin, Y.; Ling, X.; Smith, D. R.; Kong, J.; Mikkelsen, M. H. Leveraging Nanocavity Harmonics for Control of Optical Processes in 2D Semiconductors. *Nano Lett.* **2015**, *15*, 3578−3584.
(44) Lepeshov, S.; Wang, M.; Krasnok, A.; Kotov, O.; Zhang, T.; Liu, H.; Jiang, T.; Korgel, B.; Terrones, M.; Zheng, Y.; Alu, A. Tunable Resonance Coupling in Single Si Nanoparticle-Monolayer WS_2 Structures. *ACS Appl. Mater. Interfaces* **2018**, *10*, 16690−16697.
(45) Li, B.; He, Y.; Lei, S.; Najmaei, S.; Gong, Y.; Wang, X.; Zhang, J.; Ma, L.; Yang, Y.; Hong, S.; Hao, J.; Shi, G.; George, A.; Keyshar, K.; Zhang, X.; Dong, P.; Ge, L.; Vajtai, R.; Lou, J.; Jung, Y. J.; Ajayan, P. M. Scalable Transfer of Suspended Two-Dimensional Single Crystals. *Nano Lett.* **2015**, *15*, 5089−5097.

https://doi.org/10.1021/acsami.1c10295
ACS Appl. Mater. Interfaces XXXX, XXX, XXX−XXX